Article

Ground- and Excited-State Electronic Structure of an Emissive Pyrazine-Bridged Ruthenium(II) Dinuclear Complex

Wesley R. Browne, Noel M. O'Boyle, William Henry, Adrian L. Guckian, Sabine Horn, Thomas Fett, Christine M. O'Connor, Marco Duati, Luisa De Cola, Colin G. Coates, Kate L. Ronayne, John J. McGarvey, and Johannes G. Vos

J. Am. Chem. Soc., **2005**, 127 (4), 1229-1241• DOI: 10.1021/ja046034e • Publication Date (Web): 08 January 2005

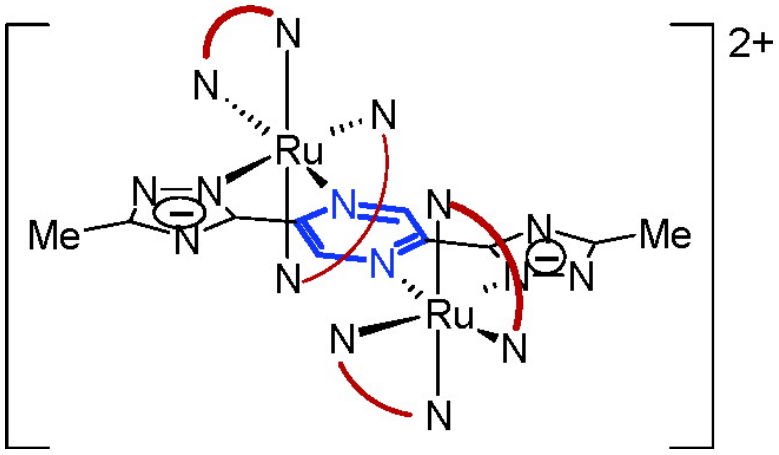

More About This Article

Additional resources and features associated with this article are available within the HTML version:

- Supporting Information
- Links to the 4 articles that cite this article, as of the time of this article download
- Access to high resolution figures
- Links to articles and content related to this article
- Copyright permission to reproduce figures and/or text from this article

View the Full Text HTML

J|A|C|S
ARTICLES
Published on Web 01/08/2005

Ground- and Excited-State Electronic Structure of an Emissive Pyrazine-Bridged Ruthenium(II) Dinuclear Complex

Wesley R. Browne,[†,||] Noel M. O'Boyle,[†] William Henry,[†] Adrian L. Guckian,[†] Sabine Horn,[†] Thomas Fett,[†] Christine M. O'Connor,[‡] Marco Duati,[§] Luisa De Cola,[§] Colin G. Coates,[⊥] Kate L. Ronayne,[⊥] John J. McGarvey,[⊥] and Johannes G. Vos*[,†]

Contribution from the National Centre for Sensor Research, School of Chemical Sciences, Dublin City University, Dublin 9, Ireland, School of Chemistry, Dublin Institute of Technology, Kevin Street, Dublin 8, Ireland, HIMS, Universiteit van Amsterdam, Nieuwe Achtergracht 166, 1018 WV Amsterdam, The Netherlands, and School of Chemistry, Queen's University Belfast, Belfast BT9 5AG, Northern Ireland

Received July 3, 2004; E-mail: Johannes.vos@dcu.ie

Abstract: The synthesis, characterization, and electrochemical, photophysical, and photochemical properties of the binuclear compounds $[(Ru(H_8\text{-bpy})_2)_2((Metr)_2Pz)](PF_6)_2$ (**1**) and $[(Ru(D_8\text{-bpy})_2)_2((Metr)_2Pz)](PF_6)_2$ (**2**), where bpy is 2,2′-bipyridine and $H_2(Metr)_2Pz$ is the planar ligand 2,5-bis(5′-methyl-4′*H*-[1,2,4]triaz-3′-yl)-pyrazine, are reported. Electrochemical and spectro-electrochemical investigations indicate that the ground-state interaction between each metal center is predominantly electrostatic and in the mixed-valence form only a low level of ground-state delocalization is present. Resonance Raman, transient, and time-resolved spectroscopies enable a detailed assignment to be made of the excited-state photophysical properties of the complexes. Deuteriation is employed to both facilitate spectroscopic characterization and investigate the nature of the lowest excited states.

Introduction

Since the first report on the paradigm pyrazine (pz)-bridged binuclear ruthenium(II) complex ($[(NH_3)_5Ru)_2pz]^{2+}$), by Creutz and Taube,[1] pyrazine-bridged multinuclear complexes have received considerable attention.[2] Investigations have focused predominantly on the electrochemical and spectroelectrochemical properties of these complexes, in particular toward the measurement of the degree of delocalization in the mixed-valence ($Ru^{II}Ru^{III}$) species.[2,3] The many structural analogues of the Creutz−Taube (CT) ion, involving substitution of the monodentate amine groups with pyridyl, bipyridyl, chloro, and/or aquo groups, have provided considerable insight into the factors that control internuclear interaction in the Ru(II)Ru(III) state.[4,5] An alternative approach to the perturbation of the ground-state properties of the CT ion has been to modify the bridging pyrazine unit by substitution in the 2,3-, 2,5-, or 2,3,5,6-positions.[6] Many of these systems are especially suited for study by techniques such as electrochemistry, spectro-electrochemistry,[7] and infrared,[8] Mössbauer,[9] and UV−vis absorption

[†] Dublin City University.
[‡] Dublin Institute of Technology.
[§] Universiteit van Amsterdam.
[⊥] Queen's University Belfast.
[||] Present address: Organic and Molecular Inorganic Chemistry, Rijksuniversiteit Groningen, Nijenborgh 4, Groningen, The Netherlands.

(1) Creutz, C.; Taube, H. *J. Am. Chem. Soc.* **1969**, *91*, 3988−3989.
(2) (a) Chen, P.; Meyer, T. J. *Chem. Rev.* **1998**, *98*, 1439−1477. (b) Brunschwig, B. S.; Creutz, C.; Sutin, N. *Chem. Soc. Rev.* **2002**, *31*, 168−184. (c) Demadis, K. D.; Hartshorn, C. M.; Meyer, T. J. *Chem. Rev.* **2001**, *101*, 2655−2685.
(3) (a) Londergan, C. H.; Kubiak, C. P. *J. Phys. Chem A.* **2003**, *107*, 9301−9311. (b) Braun-Sand, S. B.; Wiest, O. *J. Phys. Chem. A* **2003**, *107*, 285−291.
(4) (a) Callahan, R. W.; Brown G. M.; Meyer, T. J. *J. Am. Chem. Soc.* **1974**, *96*, 7829−7830. (b) Callahan, R. W.; Brown, G. M.; Meyer, T. J. *Inorg. Chem.* **1975**, *14*, 1443−1452. (c) Tom, G. M.; Creutz, C.; Taube, H. *J. Am. Chem. Soc.* **1974**, *96*, 7827−7829. (d) Meyer, T. J. *Acc. Chem. Res.* **1978**, *11*, 94−100. (e) Meyer, T. J. *Chem. Phys. Lett.* **1979**, *64*, 417−420.
(5) (a) Callahan, R. W.; Keene, F. R.; Meyer, T. J.; Salmon, D. J. *J. Am. Chem. Soc.* **1977**, *99*, 1064−1073. (b) Powers, M. J.; Meyer, T. J. *J. Am. Chem. Soc.* **1980**, *102*, 1289−1297. (c) Demadis, K. D.; Neyhart, G. A.; Kober, E. M.; White, P. S.; Meyer, T. J. *Inorg. Chem.* **1999**, *38*, 5948−5959. (d) Powers, M. J.; Meyers, T. J. *Inorg. Chem.* **1978**, *17*, 2955−2958.
(6) (a) Sarker, B.; Laye, R. H.; Mondal, B.; Chakraborty, S.; Paul, R. L.; Jeffery, J. C.; Puranik, V. G.; Ward, M. D.; Lahiri, G. K. *J. Chem. Soc., Dalton Trans.* **2002**, 2097−2101. (b) Brady, I.; Leane, D.; Hughes, H. P.; Forster, R. J.; Keyes, T. E. *J. Chem. Soc., Dalton Trans.* **2004**, 334−341. (c) Braunstein, C. H.; Baker, A. D.; Strekas, T. C.; Gafney, H. D. *Inorg. Chem.* **1984**, *23*, 857−864. (d) Richter, M. M.; Jensen, G. E.; Brewer, K. J. *Inorg. Chim. Acta* **1995**, *230*, 35−40. (e) Sherborne, J.; Scott, S. M.; Gordon, K. C. *Inorg. Chim. Acta* **1997**, *260*, 199−205. (f) Su, H. Q.; Kincaid, J. R. *J. Raman Spectrosc.* **2003**, *34*, 907−916 and references therein. (g) Marcaccio, M.; Paolucci, F.; Paradisi, C.; Roffia, S.; Fontanesi, C.; Yellowlees, L. J.; Serroni, S.; Campagna, S.; Balzani, V. *J. Am. Chem. Soc.* **1999**, *121*, 10081−10091. (h) Loiseau, F.; Serroni, S.; Campagna, S. *Collect. Czech. Chem. Commun.* **2003**, *68*, 1677−1686. (i) Marcaccio, M.; Paolucci, F.; Paradisi, C.; Carano, M.; Roffia, S.; Fontanesi, C.; Yellowlees, L. J.; Serroni, S.; Campagna, S.; Balzani, V. *J. Electroanal. Chem.* **2002**, *532*, 99−112. (j) Campagna, S.; Serroni, S.; Puntoriero, F.; Loiseau, F.; De Cola, L.; Kleverlaan, C. J.; Becher, J.; Sørensen, A. P.; Hascoat, P.; Thorup, N. *Chem. Eur. J.* **2002**, *8*, 4461−4469. (k) Swavey, S.; Brewer, K. J. *Inorg. Chem.* **2002**, *41*, 4044−4050. (l) Baudin, H. B.; Davidsson, J.; Serroni, S.; Juris, A.; Balzani, V.; Campagna, S.; Hammarström, L. *J. Phys. Chem. A* **2002**, *106*, 4312−4319. (m) Seneviratne, D. S.; Uddin, J.; Swayambunathan, V.; Schlegel, H. B.; Endicott, J. F. *Inorg. Chem.* **2002**, *41*, 1502−1517. (n) Constable, E. C.; Eriksson, H.; Housecroft, C. E.; Kariuki, B. M.; Nordlander, E.; Olsson, J. *Inorg. Chem. Commun.* **2001**, *4*, 749−752. (o) Carano, M.; Ceroni, P.; Fontanesi, C.; Marcaccio, M.; Paolucci, F.; Paradisi, C.; Roffia, S. *Electrochim. Acta* **2001**, *46*, 3199−3206. (p) Puntoriero, F.; Serroni, S.; Licciardello, A.; Venturi, M.; Juris, A.; Ricevuto, V.; Campagna, S. *J. Chem. Soc., Dalton Trans.* **2001**, 1035−1042. (q) Goldsby K. A.; Meyer, T. J. *Inorg. Chem.* **1984**, *23*, 3002−3010.
(7) (a) Yeomans, B. D.; Kelso, L. S.; Tregloan, P. A.; Keene, F. R. *Eur. J. Inorg. Chem.* **2001**, 239−246. (b) D'Alessandro, D. M.; Kelso, L. S.; Keene, F. R. *Inorg. Chem.* **2001**, *40*, 6841−6844.

spectroscopies. The majority of these studies have focused on the relative delocalization of the SOMO, in the mixed-valence form, over the metal centers and the mechanism for interaction in systems where direct overlap of the metal orbitals is not possible (i.e., superexchange processes mediated via either the HOMO or the LUMO of the bridging ligand). The results of these studies can be extended, albeit tentatively, as a guide to the level of excited-state communication between the molecular components in large systems in their homovalent states (i.e., $Ru^{II}Ru^{II}$), and while this extrapolation may give an indication of the level of excited-state interaction, it assumes that the bridging ligand provides the same contribution toward internuclear interaction in the mixed-valence state as in the homovalent excited state. This assumption fails, however, when the LUMO of the bridging ligand provides a significant contribution to the lowest excited states, or the dominant mechanism for energy transfer is via a through-space (Förster) rather than a through-bond (Dexter) energy-transfer mechanism.[10] It is surprising then that, despite such a significant level of interest, the photochemical and excited-state properties of pyrazine-bridged complexes have received relatively little attention, with the notable exception of the dipyridopyrazine (dpp)-based family of complexes.[6,11]

In the present contribution, the effect of the introduction of a pH-sensitive 1,2,4-triazole moiety on the ground- and excited-state properties of a pyrazine-bridged binuclear Ru(II) complex is examined in the synthesis and characterization of the binuclear complexes $[(Ru(H_8\text{-bpy})_2)_2((Metr)_2Pz)](PF_6)_2$ (**1**) and $[(Ru(D_8\text{-bpy})_2)_2((Metr)_2Pz)](PF_6)_2$ (**2**), where bpy is 2,2′-bipyridine and $H_2(Metr)_2Pz$ is 2,5-bis(5′-methyl-4′*H*-[1,2,4]triaz-3′-yl)pyrazine (Figure 1). Recently, a series of ditopic ligands containing both pyrazine and 1,2,4-triazole moieties have been reported (Figure 2).[10] The primary interest in such mixed electron acceptor/electron donor ligands is in the ability to tune, independently, ground- and excited-state properties in multinuclear complexes.[10] In addition, the acid−base chemistry of the bridging triazole moiety influences strongly the properties of the complexes.[10,12−14]

Of particular interest in the present study is the effect of the protonation state of the nonbridging 1,2,4-triazole on the degree of internuclear communication and on photophysical properties. Extensive resonance Raman spectroscopic investigations of both the ground and lowest excited electronic states, together with computational analysis (DFT), enable a detailed model of the excited-state electronic structure to be developed. The results obtained are compared with those reported for related ligand systems, e.g., Hbpzt[15] and H_2bisztr,[10b] where Hbpzt is 2-(3-pyrazin-2-yl-1*H*-1,2,4-triazol-5-yl)pyrazine and H_2bispztr is 5,5′-dipyrazin-2-yl-1*H*,1′*H*-3,3′-bi-1,2,4-triazole (Figure 2). A de-

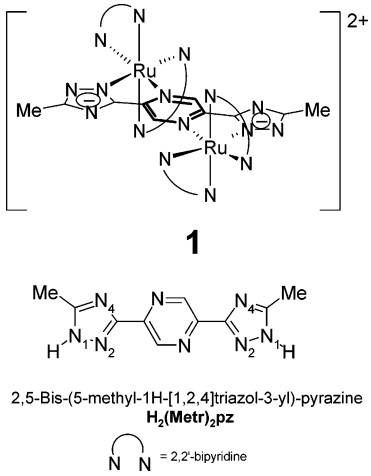

Figure 1. Structure of the ligand $H_2(Metr)_2pz$ and complex **1**.

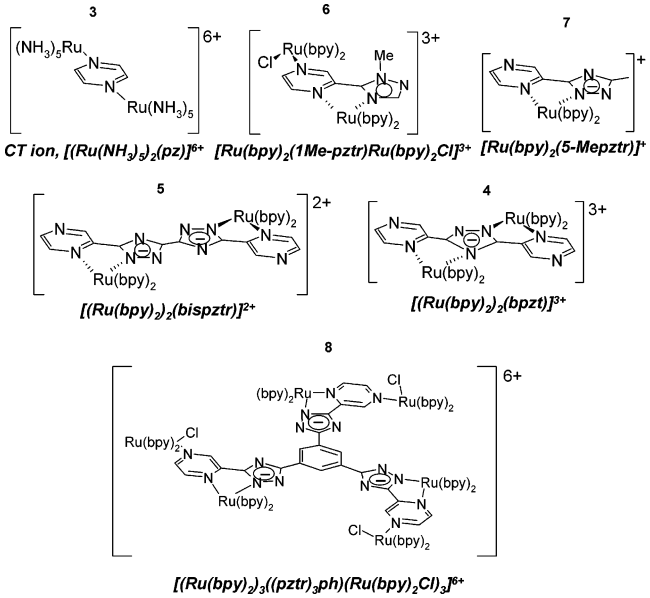

Figure 2. Structure of some of the complexes discussed in the text.

(8) (a) Dattelbaum, D. M.; Hartshorn, C. M.; Meyer, T. J. *J. Am. Chem. Soc.* **2002**, *124*, 4938−4939. (b) Crayston, J. A.; Cupertino, D. C.; Dines, T. J. *J. Chem. Soc., Dalton Trans.* **1991**, 1603−1608. (c) Toma, H. E.; Santos, P. S. *Can. J. Chem.* **1977**, *55*, 3549−3553. (d) Londergan, C. H.; Salsman, J. C.; Ronco, S.; Kubiak, C. P. *Inorg. Chem.* **2003**, *42*, 926−928.

(9) Fürholz, U.; Bürgi, H.-B.; Wagner, F. E.; Stebler, A.; Ammeter, J. H.; Krausz, E.; Clark, R. J. H.; Stead, M. J.; Ludi, A. *J. Am. Chem. Soc.* **1984**, *106*, 121−123.

(10) (a) Browne, W. R.; Weldon, F.; Guckian, A.; Vos, J. G. *Collect. Czech. Chem. Commun.* **2003**, *68*, 1467−1487. (b) Di Pietro, C.; Serroni, S.; Campagna, S.; Gandolfi, M. T.; Ballardini, R.; Fanni, S.; Browne, W. R.; Vos J. G. *Inorg. Chem.* **2002**, *41*, 2871−2878. (c) Weldon, F.; Hammarström, L.; Mukhtar, E.; Hage, R.; Gunneweg, E.; Haasnoot, J. G.; Reedijk, J.; Browne, W. R.; Guckian, A. L.; Vos J. G. *Inorg. Chem.* **2004**, *43*, 4471−4481.

(11) (a) Fuchs, Y.; Lofters, S.; Dieter, T.; Shi, W.; Morgan, R.; Strekas, T. C.; Gafney, H. D.; Baker, A. D. *J. Am. Chem. Soc.* **1987**, *109*, 2691−2697. (b) Scott, S. M.; Gordon, K. C. *Inorg. Chim. Acta* **1997**, *254*, 267−272. (c) Cooper, J. B.; MacQueen, D. B.; Petersen, J. D.; Wertz, D. W. *Inorg. Chem.* **1990**, *29*, 3701−3705.

(12) (a) Hage, R.; Prins, R.; Haasnoot, J. G.; Reedijk, J.; Vos, J. G. *J. Chem. Soc., Dalton Trans.* **1987**, 1389−1395. (b) Nieuwenhuis, H. A.; Haasnoot, J. G.; Hage, R.; Reedijk, J.; Snoeck, T. L.; Stufkens, D. J.; Vos, J. G. *Inorg. Chem.* **1991**, *30*, 48−54. (c) Buchanan, B. E.; Wang, R.; Vos, J. G.; Hage, R.; Haasnoot, J. G.; Reedijk, J. *Inorg. Chem.* **1990**, *29*, 3263−3265. (d) Browne, W. R.; O'Connor, C. M.; Villani, C.; Vos, J. G. *Inorg. Chem.* **2001**, *40*, 5461−5464. (e) Hage, R.; Haasnoot, J. G.; Nieuwenhuis, H. A.; Reedijk, J.; de Ridder, D. J. A.; Vos, J. G. *J. Am. Chem. Soc.* **1990**, *112*, 9245−9254. (f) de Wolf, J. M.; Hage, R.; Haasnoot, J. G.; Reedijk, J.; Vos, J. G. *New J. Chem.* **1991**, *15*, 501−507. (g) Hage, R.; Dijkhuis, A. H. J.; Haasnoot, J. G.; Prins, R.; Reedijk, J.; Buchanan B. E.; Vos, J. G. *Inorg. Chem.* **1988**, *27*, 2185−2189.

(13) (a) Barigelletti, F.; De Cola, L.; Balzani, V.; Hage, R.; Haasnoot, J. G.; Reedijk, J.; Vos, J. G. *Inorg.* Chem. **1989**, *28*, 4344−4350. (b) van Diemen, J. H.; Hage, R.; Haasnoot, J. G.; Lempers, H. E. B.; Reedijk, J.; Vos, J. G.; de Cola, L.; Barigelletti, F.; Balzani, V. *Inorg. Chem.* **1992**, *31*, 3518−3522. (c) Barigelletti, F.; De Cola, L.; Balzani, V.; Hage, R.; Haasnoot, J. G.; Reedijk, J.; Vos, J. G. *Inorg. Chem.* **1991**, *30*, 641−645. (d) Passaniti, P.; Browne, W. R.; Lynch, F. C.; Hughes, D.; Nieuwenhuyzen, M.; James, P.; Maestri, M.; Vos, J. G. *J. Chem. Soc., Dalton Trans.* **2002**, 1740−1476. (e) Hage, R.; Lempers, H. E. B.; Haasnoot, J. G.; Reedijk, J.; Weldon, F. M.; Vos, J. G. *Inorg. Chem.* **1997**, *36*, 3139−3145.

(14) (a) Coates, C. G.; Keyes, T. E.; Hughes, H. P.; Jayaweera, P. M.; McGarvey, J. J.; Vos, J. G. *J. Phys. Chem. A* **1998**, *102*, 5013−5018. (b) Hage, R.; Haasnoot, J. G.; Stufkens, D. J.; Snoeck, T. L.; Vos, J. G.; Reedijk, J. *Inorg. Chem.* **1989**, *28*, 1413−1414. (c) Keyes, T. E.; O'Connor, C. M.; O'Dwyer, U.; Coates, C. G.; Callaghan, P.; McGarvey, J. J.; Vos, J. G. *J. Phys. Chem. A* **1999**, *103*, 8915−8920.

(15) Hage, R.; Haasnoot, J. G.; Reedijk, J.; Wang, R.; Vos, J. G. *Inorg. Chem.* **1991**, *30*, 3263−3269.

tailed picture of the excited-state electronic structure is described, and the influence of energy states lying higher than the lowest emissive state is discussed.

Experimental Section

Materials. All solvents employed were of HPLC grade or better and used as received. For all spectroscopic measurements, Uvasol (Merck)-grade solvents were employed. All reagents employed in synthetic procedures were of reagent grade or better. 2,2′-Bipyridine (Aldrich) and [*cis*-[Ru([D_8]-bpy)$_2$Cl$_2$]·2H$_2$O (Complex-Solutions, Dublin, Ireland) were used as received. *cis*-[Ru(bpy)$_2$Cl$_2$]·2H$_2$O,[16] pyrazine-2,5-dicarbonitrile,[17] and tetraethylammonium perchlorate (TEAP)[18] were prepared by previously reported procedures. The synthesis of the ligand, 2,5-bis(5′-methyl-4′*H*-[1,2,4]triaz-3′-yl)pyrazine {H$_2$(Metr)$_2$pz}, was carried out according to literature methods.[12] ^{1}H NMR in DMSO-d_6: δ 9.41 (2H, s), 2.79 (6H, s). Preparation of the dinuclear complexes was by direct reaction of the ligand with 2 equiv of *cis*-[Ru(bpy)$_2$Cl$_2$] or *cis*-[Ru([D_8]-bpy)$_2$Cl$_2$], with purification by column chromatography on neutral alumina. Both complexes gave satisfactory mass spectra, which showed isotopic patterns in agreement with calculated spectra. Detailed synthetic procedures are available as Supporting Information.

[(Ru(bpy)$_2$)$_2$((Metr)$_2$Pz)](PF$_6$)$_2$·3H$_2$O (1). This compound was recrystallized from neutral solution, and therefore the triazole units are deprotonated. ^{1}H NMR spectroscopy (in CD$_3$CN/NaOD): δ 8.52 (m, 3H), 8.44 (m, 5H), 8.175 (d, 1H), 8.12 (m, 4H), 8.05 (d, 1H), 7.99 (m, 6H), 7.89 (d, 1H), 7.75 (d, 1H), 7.68 (d, 1H), 7.64 (m, 2H), 7.51 (m, 5H), 7.35 (m, 3H), 7.175 (dd, 1H), 2.18 (s, methyl, 3H), 2.175 (s, methyl, 3H). Mass spectroscopy: Mol^{2+} (calcd for C$_{50}$H$_{40}$N$_{16}$Ru$_2$, 534) found, 534 *m*/*z*. Elemental analysis (calcd for C$_{50}$H$_{40}$N$_{16}$RuP$_2$F$_{12}$·3H$_2$O): C 42.64 (42.55), H 2.75 (3.05), N 15.64 (15.89).

[(Ru([D_8]-bpy)$_2$)$_2$(H$_2$(Metr)$_2$Pz)](PF$_6$)$_4$ (2). This compound was obtained from acidic solution, and therefore the triazole groups are protonated. ^{1}H NMR spectroscopy (in CD$_3$CN/NaOD): δ 7.98 (s, 1H), 7.92 (s, 1H), 2.18 (s, methyl, 3H), 2.175 (s, methyl, 3H). Mass spectroscopy: Mol^{2+} (calcd for C$_{50}$D$_{32}$H$_8$N$_{16}$Ru$_2$, 550) found, 550 *m*/*z*. Elemental analysis (calcd for C$_{50}$H$_{10}$D$_{32}$N$_{16}$RuP$_4$F$_{24}$): C 36.10 (35.71), H 2.38 (2.5), N 13.00 (13.33).

Physical Measurements. ^{1}H NMR, UV−vis, emission and mass spectra, luminescence lifetime, electrochemical and spectro-electrochemical measurements,[12d] transient differential absorption spectroscopy,[19] resonance Raman, and transient and time-resolved resonance Raman (TR^2 and TR^3)[14c,20] were carried out as reported elsewhere and are described in detail in the Supporting Information. Photolysis experiments were carried out at room temperature in acetonitrile using visible light with a 400-W tungsten filament light source. Elemental analysis was carried out at the Micro-analytical Laboratory at University College Dublin.

Density Functional Theory Calculations. Density functional calculations were carried out with Gaussian 03W[21] using Becke's three-parameter hybrid functional[22] with the LYP correlation functional[23] (B3LYP). The LanL2DZ basis set was used. This uses the Dunning−Huzinaga double-ζ basis functions[24] (DZ) for carbon, nitrogen, and hydrogen atoms, the Los Alamos effective core potential for the Ru core electrons, and DZ functions for the Ru valence electrons.[25] An ultrafine integration grid was used. The structures of the heterochiral isomers of **1** and **H$_2$1** were constrained to C_i symmetry during the geometry optimization. The energies and intensities of the 35 lowest energy singlet−singlet electronic transitions were calculated at the optimized geometry using TD-DFT. GaussSum 0.8[26] was used to calculate group contributions to the molecular orbitals, to prepare the partial density of states (PDOS) spectra, to convolute the calculated UV−vis spectrum, and to prepare the electron density difference maps (EDDMs). The contribution of a group to a molecular orbital was calculated within the framework of Mulliken population analysis. The PDOS spectra were created by convoluting the molecular orbital information with Gaussian curves of unit height and fwhm of 0.3 eV. The UV−vis spectrum was convoluted with Gaussian curves of fwhm of 3000 cm^{-1}.

Results

^{1}H NMR Spectroscopy. ^{1}H NMR data are given in the Experimental Section and in the Supporting Information, Figure S1. For **1**, two methyl resonances at 2.175 and 2.18 ppm and a total of 34 aromatic resonances are observed, while for the [D_8]-bpy analogue **2** only the resonances due to the methyl groups and pyrazine ring are observed, as expected. The observation of two methyl and two pyrazine singlet resonances is explained by the presence of two diastereoisomeric forms for both compounds (i.e., $\Delta\Delta/\Lambda\Lambda$ and $\Lambda\Delta$) and confirms that the coordination mode of each of the 1,2,4-triazole rings is the same (i.e., N2N2 or N4N4 and not N2N4, see Figure 1).[12d,27]

The incorporation of a methyl substituent in the C5 position of the 1,2,4-triazole ring is known to inhibit coordination via the N4 of the 1,2,4-triazole ring, resulting in almost exclusive formation of the N2-bound isomer (>90%).[12a,13,28] The methyl ^{1}H NMR resonance of the 1,2,4-triazole ring is particularly sensitive to the coordination mode of the ring. In the related mononuclear complexes, [Ru(LL)$_2$(5-Mepztr)]$^+$ (where LL = bpy, phen, or dmbpy, Figure 2),[28] a resonance at 2.15−2.35 ppm is indicative of N2 coordination, while for N4 coordination an upfield shift in the methyl resonance to 1.1−1.3 ppm is observed, due to through-space interaction with a neighboring polypyridyl ligand. The methyl resonance observed at 2.18 ppm for the compounds reported in this contribution, therefore, confirms the N2N2 coordination mode to the 1,2,4-triazole rings.

(16) Sullivan, B. P.; Salmon, D. J.; Meyer, T. J. *Inorg. Chem.* **1978**, *17*, 3334−3341.
(17) Suenaga, Y.; Kamiya, T.; Kuroda-Sowa, T.; Maekawa, M.; Munakata, M. *Inorg. Chim. Acta* **2000**, *308*, 17−21.
(18) Wang, R.; Vos, J. G.; Schmehl, R. H.; Hage, R. *J. Am. Chem. Soc.* **1992**, *114*, 1964−1970.
(19) (a) Kleverlaan, C. J.; Stufkens, D. J.; Clark, I. P.; George, M. W.; Turner, J. J.; Martino, D. M.; van Willigen, H.; Vlček, A., Jr. *J. Am. Chem. Soc.* **1998**, *120*, 10871−10879. (b) Staffilani, M.; Peter Belser, P.; Hartl, F.; Kleverlaan, C. J.; Luisa De Cola, L. *J. Phys. Chem. A* **2002**, *106*, 9242−9250.
(20) (a) Coates, C. G.; Jacquet, L.; McGarvey, J. J.; Bell, S. E. J.; Al-Obaidi, A. H. R.; Kelly, J. M. *J. Am. Chem. Soc.* **1997**, *119*, 7130−7136. (b) Coates, C. G.; Olofsson, J.; Coletti, M.; McGarvey, J. J.; Önfelt, B.; Lincoln, P.; Norden, B.; Tuite, E.; Matousek, P.; Parker, A. W. *J. Phys. Chem. B* **2001**, *105*, 12653−12664.
(21) Frisch, M. J.; Trucks, G. W.; Schlegel, H. B.; Scuseria, G. E.; Robb, M. A.; Cheeseman, J. R.; Montgomery, J. A., Jr.; Vreven, T.; Kudin, K. N.; Burant, J. C.; Millam, J. M.; Iyengar, S. S.; Tomasi, J.; Barone, V.; Mennucci, B.; Cossi, M.; Scalmani, G.; Rega, N.; Petersson, G. A.; Nakatsuji, H.; Hada, M.; Ehara, M.; Toyota, K.; Fukuda, R.; Hasegawa, J.; Ishida, M.; Nakajima, T.; Honda, Y.; Kitao, O.; Nakai, H.; Klene, M.; Li, X.; Knox, J. E.; Hratchian, H. P.; Cross, J. B.; Adamo, C.; Jaramillo, J.; Gomperts, R.; Stratmann, R. E.; Yazyev, O.; Austin, A. J.; Cammi, R.; Pomelli, C.; Ochterski, J. W.; Ayala, P. Y.; Morokuma, K.; Voth, G. A.; Salvador, P.; Dannenberg, J. J.; Zakrzewski, V. G.; Dapprich, S.; Daniels, A. D.; Strain, M. C.; Farkas, O.; Malick, D. K.; Rabuck, A. D.; Raghavachari, K.; Foresman, J. B.; Ortiz, J. V.; Cui, Q.; Baboul, A. G.; Clifford, S.; Cioslowski, J.; Stefanov, B. B.; Liu, G.; Liashenko, A.; Piskorz, P.; Komaromi, I.; Martin, R. L.; Fox, D. J.; Keith, T.; Al-Laham, M. A.; Peng, C. Y.; Nanayakkara, A.; Challacombe, M.; Gill, P. M. W.; Johnson, B.; Chen, W.; Wong, M. W.; Gonzalez, C.; Pople, J. A. *Gaussian 03*, Revision B.04; Gaussian, Inc.: Pittsburgh PA, 2003.
(22) Becke, A. D. *J. Chem. Phys.* **1993**, *98*, 5648−5652.
(23) Lee, C.; Yang, W.; Parr, R. G. *Phys. Rev. B* **1988**, *37*, 785−789.
(24) Dunning, T. H., Jr.; Hay, P. A. In *Modern Theoretical Chemistry*; Schaefer, H. F., III, Ed.; Plenum: New York, 1977; Vol. 3, p 1.
(25) (a) Hay, P. J.; Wadt, W. R. *J. Chem. Phys.* **1985**, *82*, 270−283. (b) Wadt, W. R.; Hay, P. J. *J. Chem. Phys.* **1985**, *82*, 284−298. (c) Hay, P. J.; Wadt, W. R. *J. Chem. Phys.* **1985**, *82*, 299−310.
(26) O'Boyle, N. M.; Vos, J. G. *GaussSum 0.8*; Dublin City University, 2003.
(27) Baitalik, S.; Bag, P.; Flörke, U.; Nag, K. *Inorg. Chim. Acta* **2004**, *357*, 699−706.
(28) Ryan, E. M.; Wang, R.; Vos J. G.; Hage, R.; Haasnoot, J. G. *Inorg. Chim. Acta* **1993**, *208*, 49−58.

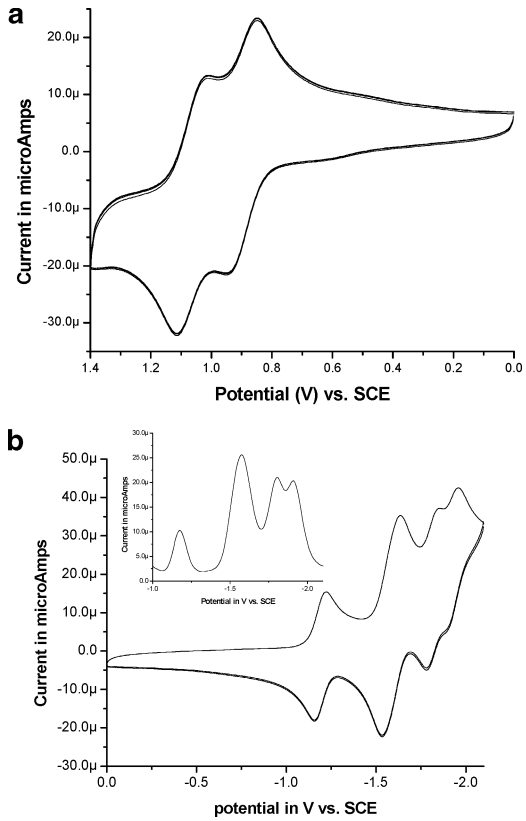

Figure 3. (a) Metal-based oxidation. (b) Ligand-based processes for **1** in 0.1 M TEAP/CH_3CN (CV scan rate 200 mV s^{-1}; inset, DPV scan rate 40 mV s^{-1}).

Redox, Electronic, Photochemical, and Acid−Base Properties. Reversible metal-based oxidation processes are observed at 0.875 and 1.05 V (vs SCE, Figure 3) for **1** and at 1.28 and 1.45 V for $\mathbf{H_21}$. The first oxidation process occurs at potentials comparable with those observed for related 1,2,4-triazole-based complexes but at a considerably higher potential than observed for the Creutz−Taube ion (see Table 1). For **1**, four reversible reduction processes are observed between −1.0 and −2.0 V. Due to the electron-deficient nature of the pyrazine ring, the first reduction process is expected to be pyrazine-based, followed by bpy-based reductions.[11c]

The separation of the first and second oxidation processes facilitates the preparation of the mixed-valence and fully oxidized complexes by bulk electrolysis, and although the complex becomes unstable in the II/III and III/III oxidation states,[6c,29] useful information may still be obtained using this technique. For $\mathbf{H_21}$ only a very weak band is observed at ∼850 nm upon oxidation at 1.0 V. Oxidation at a potential above the second oxidation wave results in a depletion of this feature, which suggests that it is an intervalence (IT) band. For **1**, evidence for the presence of an IT band (between 400 and 2500 nm) was not obtained by either spectroelectrochemistry or chemical oxidation.

The absorption spectrum of **1** shows strong absorption features at ∼550 and ∼450 nm (Figure 4), which are assigned to metal-to-ligand-charge-transfer transitions (^{1}MLCT). An equally intense absorption feature at ∼350 nm (vide infra) and a very intense absorption band at ∼280 nm are assigned as intraligand ($\pi-\pi^*$) transitions (Table 1).[30] Figure 4 shows that there are two different protonation steps, indicating significant interaction between the two triazole rings, and as a result the formation of the singly protonated **H1** is observed at intermediate pH values. Protonation results in a red shift of the lowest absorption band from 530 to 565 nm, while the higher energy band undergoes a blue shift from 467 to 424 nm. The intraligand ($\pi-\pi^*$) transition at ∼280 nm undergoes only a relatively minor blue shift on protonation; however, the absorption band at ca. 350 nm is more strongly blue-shifted. The pK_a values for the two protonation steps are pK_{a1} = 2.7 and pK_{a2} = 4.7 ± 0.1.

$$\mathbf{H_21} \overset{pK_{a1}=2.7}{\rightleftharpoons} \mathbf{H1} \overset{pK_{a2}=4.7}{\rightleftharpoons} \mathbf{1}$$

The absorption and the emission spectra of $\mathbf{1}/\mathbf{H_21}$ exhibit solvatochromic behavior. Interestingly, the effects of solvent on each of the absorption bands are different. For both **1** and $\mathbf{H_21}$, the lowest energy band undergoes a red shift with increasing solvent polarity, while the bands at ca. 450 and 350 nm are blue-shifted. Both **1** and $\mathbf{H_21}$ are emissive at room temperature and at 77 K (Table 1), and although the emission spectra are unaffected by deuteriation of the bpy ligands, deuteriation has a noticeable effect on the emission lifetime of the complexes (Table 1). At 298 K, deuteriation results in an increase in emission lifetime of ca. 17%, while at 77 K, the effect is more pronounced, with an increase in emission lifetime of 30%. Upon protonation of **1** to form **H1** and subsequently to form $\mathbf{H_21}$, the emission spectrum of the complex undergoes a red shift from 748 nm to >800 nm (in CH_3CN),[31] and the decrease in emission lifetime is observed for $\mathbf{H_21}$ compared to **1**, in agreement with the energy gap law.[32]

The photochemical stability of **1** and $\mathbf{H_21}$ was examined in H_2O, methanol, ethanol, acetone, acetonitrile, THF, DMF, DMSO, and dichloromethane by monitoring changes in their UV−vis absorption and emission spectra during photolysis.[33] Surprisingly, for $\mathbf{H_21}$ no evidence for photodecomposition was observed after extended photolysis (4 h) in any of the solvent systems examined. Similarly, **1** was found to be photostable in protic solvents and in most aprotic solvents. However, in acetonitrile and DMSO, **1** was found to be photochemically unstable, with changes (a collapse of the absorption at 550 nm and modification of the absorption at ∼350 nm; see Supporting Information, Figure S2) observed over several minutes of irradiation.

Resonance Raman Spectroscopy.[34] Ground-state resonance Raman (rR) spectra were obtained for $\mathbf{1}/\mathbf{H_21}$ at λ_{ex} = 457.9, 488, 514.5, and 532 nm. Assignment of the spectra is facilitated greatly by the availability of the deuterated analogue $\mathbf{2}/\mathbf{H_22}$. Figure 5 shows the excitation wavelength dependence of the rR spectra between 457.9 and 532 nm for **1** in basic aqueous solution. At all wavelengths examined, features are observed at 1603, 1508, 1477, 1401, 1283, 1244, and 1165 cm^{-1}. These

(29) Adeyemi, S. A.; Braddock, J. N.; Brown, G. M.; Ferguson J. A.; Miller, F. J.; Meyer, T. J. *J. Am. Chem. Soc.* **1972**, *94*, 300−301.

(30) Milkevitch, M.; Brauns, E.; Brewer, K. J. *Inorg. Chem.* **1996**, *35*, 1737−1739.

(31) Between 800 and 850 nm the detector response drops off, and hence the true λ_{max} of emission <800 nm is not determinable.

(32) Kober, E. M.; Caspar, J. V.; Lumpkin R. S.; Meyer, T. J. *J. Phys. Chem.* **1986**, *90*, 3722−3734.

(33) Examination of the photochemistry of the monoprotonated complex was not attempted due to the small separation between the first and second protonation steps, which might have resulted in the photochemistry of any of three protonation states being observed in this pH region.

(34) Strommen, D. P.; Nakamoto, K. *J. Chem. Educ.* **1977**, *54*, 474−478.

Table 1. Redox and Spectroscopic Data for **1**/**H$_2$1** and **2**/**H$_2$2** and Related Complexes in CH_3CN (Protonation with CF_3CO_2H)

		emission λ_{max}/nm					
	absorption λ_{max}/nm (log ϵ)	τ/ns at 298 K	τ/μs at 77 K[a]	M(II)/M(III) $E_{1/2}$/V vs SCE	ligand red. $E_{1/2}$/V vs SCE	energy of IT band/ cm^{-1} (ϵ)	ref
1	241 (4.56), 290 (4.89), 467 (4.22), 530 (4.38)	748 (191)	697 (2.32)	0.875 [1], 1.05 [1]	−1.18 [1], −1.58 [2], −1.80 [1], −1.91 [1]	11 760 (<100)	
H$_2$1	282 (4.88), 424 (4.21), 565 (4.34)	780 (124)	756 (1.65)	1.28 [1], 1.45 [1]			
2	241(4.64), 290 (4.98) 467 (4.25), 530 (4.35)	749 (220)	700 (3.15)	0.875 [1], 1.05 [1]	−1.18 [1], −1.58 [2] −1.80 [1], −1.91 [1]		
H$_2$2	282 (4.80), 424 (4.24) 565 (4.33)	779 (142)	750 (2.23)	1.28 [1], 1.45 [1]			
$[(bpy)_2ClRu_2(pyrazine]^{2+}$	292 (4.96), 339 (4.08), 497, 513 (4.41)			0.89 [1], 1.02 [1]		7690 (455)	5a
4 $[((bpy)_2Ru)_2bpzt]^{3+}$	449 (4.42)	670 (106)	610 (6.4)	1.16 [1], 1.46 [1]	−1.26, −1.39, −1.55, −1.63, −1.85	5405 (2200)	15
5 $[((bpy)_2Ru)_2(bispztr)]^{2+}$	455	670 (214)		0.92 [1], 1.09 [1]		5580 (1120)	10b
H$_2$5 $[((bpy)_2Ru)_2H_2bispztr]^{4+}$	430	678 (1000)		1.13 [2]			10b
6 $[Ru(bpy)_2(1Me\text{-}pztr)\text{-}Ru(bpy)_2Cl]^{3+}$	440 (4.23), 530 (4.28)	730	705	0.92 [1], 1.41 [1]	−0.97 [1], −1.51 [1] −1.57 [1], −1.76 [1]	10 400 (480)	12e
8 $[(Ru(bpy)_2)_3((pztr)_3ph)\text{-}(Ru(bpy)_2Cl)_3]^{6+}$	465 (6.72), 515 (6.72)	775	685	0.94, 1.16	−1.14, −1.50, −1.71		49
H$_3$8 $[(Ru(bpy)_2)_3((Hpztr)_3ph)\text{-}(Ru(bpy)_2Cl)_3]^{9+}$	445 (6.35), 530 (6.50)	769	695	0.97, 1.35			49
7 $[(bpy)_2Ru(5\text{-}Mepztr)]^{+}$	458 (1.21)	670	627	0.92 [1]	−1.44, −1.66, −1.80		12b
H7 $[(bpy)_2Ru(H5\text{-}Mepztr)]^{2+}$	441 (1.27)	665	620	1.29 [1]	−1.22, −1.52, −1.77		12b
$[Ru(bpy)_3]^{2+}$	452 (4.1)	620 (1000)	582 (4.8)	1.23 [1]	−1.36, −1.54, −1.79		37
$[Ru(bpz)_3]^{2+}$	440 (4.1)	610 (740)	573	1.93 [1]	−0.74, −0.92, −1.18		35

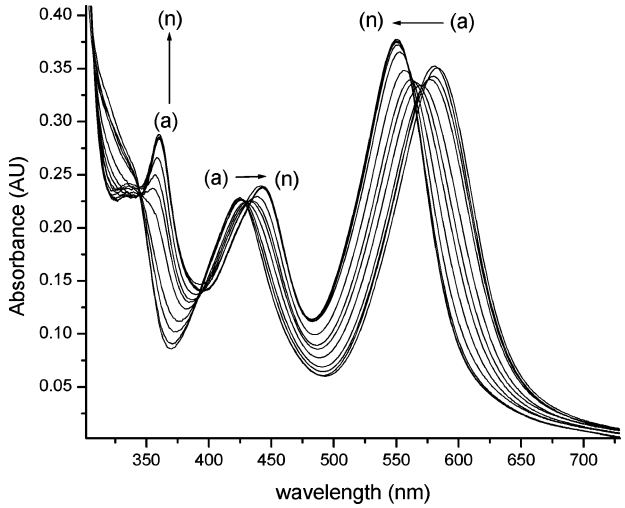

Figure 4. Absorption spectra of **1** at pH (a) 1.02, (b) 1.34, (c) 2.17, (d) 2.44, (e) 3.04, (f) 3.38, (g) 3.61, (h) 4.03, (i) 4.62, (j) 5.3, (l) 6.01, (k) 6.98, (m) 9.41, and (n) 12.98 in Britton−Robinson buffer (pH was adjusted using concentrated sulfuric acid or sodium hydroxide solution).

are assigned to pyrazine-based vibrations, based on comparison with $[Ru(bpz)_3]^{2+}$ [35] (1596, 1517, 1484, 1410 (w), 1347, 1277, 1194, 1164 cm^{-1}).[36] At 457.9 nm, and to a lesser extent at 488 nm, additional bands are observed at 1605 {1574}, 1560 {1523}, 1487 {1418}, 1318 {1255}, 1275, and 1176 cm^{-1}, which are readily assigned as bpy modes on the basis of the isotope shift observed in **2** ([D_8]-bpy band energies in {}) and by comparison with the spectrum of $[Ru(bpy)_3]^{2+}$.[37,38] A similar trend is observed for the fully protonated complex (**H$_2$1**), with bands at 1612, 1510, 1494, 1425, 1318, 1291, 1196, and 1151 cm^{-1} assigned to the protonated pyrazine ligand. Shorter-wavelength excitation shows some diminution of these bands, in parallel with the appearance of vibrational bands at 1565, 1493, 1425, 1320, and 1278 cm^{-1}, again assigned as bpy vibrations (see Supporting Information, Figure S3). It is interesting that the 1612 cm^{-1} pyrazine band retains its relative intensity at shorter-wavelength excitation, indicating that there is a significant contribution of pyrazine-based ^{1}MLCT at 457 nm.[39]

The solvent dependence of the absorption spectra and in particular the opposite dependence of the ∼450 and ∼530 nm absorption features (vide supra) has implications for the resonance Raman experiments. rR spectra recorded at 457.9 nm in CD_3CN show enhancement of the vibrational features assigned to bpy relative to those of pyrazine, compared with the spectrum obtained in H_2O (see Supporting Information, Figure S4). This is in accordance with the red shift observed in the ∼450 nm absorption band in acetonitrile relative to water, which brings the transition into better resonance with the 457.9 nm excitation line (see Figure 6 and Supporting Information, Figure S4).

Excited-State Transient Absorption and Transient Resonance Raman Spectroscopy.[40] The nanosecond transient differential absorption (ΔA) spectra of both **1** and **H$_2$1** are shown in Figure 7. For both, upon excitation at 450 nm, a pronounced bleaching of the ground-state absorption spectrum is observed, with excited-state absorption bands appearing for **1** at 380 and 480 nm and for **H$_2$1** at 365 and 475 nm. The relatively small differences in the transient absorption spectra between **1** and

(35) Allan, G. H.; White, R. P.; Rillema, D. P.; Meyer, T. J. *J. Am. Chem. Soc.* **1984**, *106*, 2613−2620.
(36) Danzer, G. D.; Kincaid, J. R. *J. Phys. Chem.* **1990**, *94*, 3976−3980.
(37) Juris, A.; Balzani, V.; Barigelletti, F.; Campagna, S.; Belser, P.; von Zelewsky, A. *Coord. Chem. Rev.* **1988**, *84*, 85−277.
(38) (a) Maruszewski, K.; Bajdor, K.; Strommen, D. P.; Kincaid, J. R. *J. Phys. Chem.* **1995**, *99*, 6286−6293. (b) Mallick, P. K.; Danzer, G. D.; Strommen, D. P.; Kincaid, J. R. *J. Phys. Chem.* **1988**, *92*, 5628−5634. (c) Strommen, D. P.; Mallick, P. K.; Danzer, G. D.; Lumpkin, R. S.; Kincaid, J. R. *J. Phys. Chem.* **1990**, *94*, 1357−1366.
(39) Gardner, J. S.; Strommen, D. P.; Szulbinski, W. S.; Su, H.; Kincaid, J. R. *J. Phys. Chem. A* **2003**, *107*, 351−357.
(40) (a) Terner, J.; El-Sayed, M. A. *Acc. Chem. Res.* **1985**, *18*, 331−338. (b) Schoonover, J. R.; Strouse, G. F. *Chem. Rev.* **1998**, *98*, 1335−1355. (c) Morris, D. F.; Woodruff, W. H. In *Spectroscopy of Inorganic Based materials*; Clark, R. J. H., Hester, R. E., Eds.; John Wiley & Sons: New York, 1987.

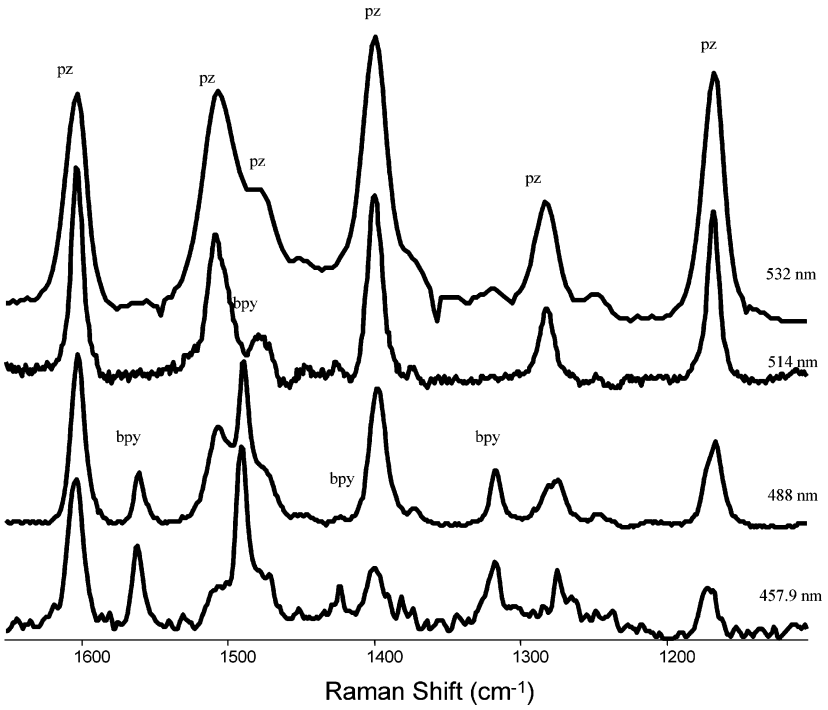

Figure 5. Resonance Raman spectra of **1** in H_2O at 457.9, 488, 514, and 532 nm probe wavelengths.

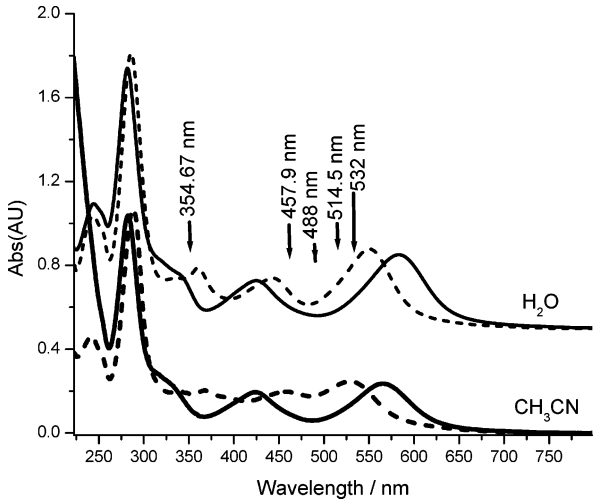

Figure 6. Absorption spectra of **1** (dashed line) and $\mathbf{H_21}$ (solid line) in H_2O (top) and CH_3CN (bottom). Spectra in H_2O are offset by 0.5 AU for clarity. λ_{exc} values used in recording ground- and excited-state resonance Raman spectra are indicated.

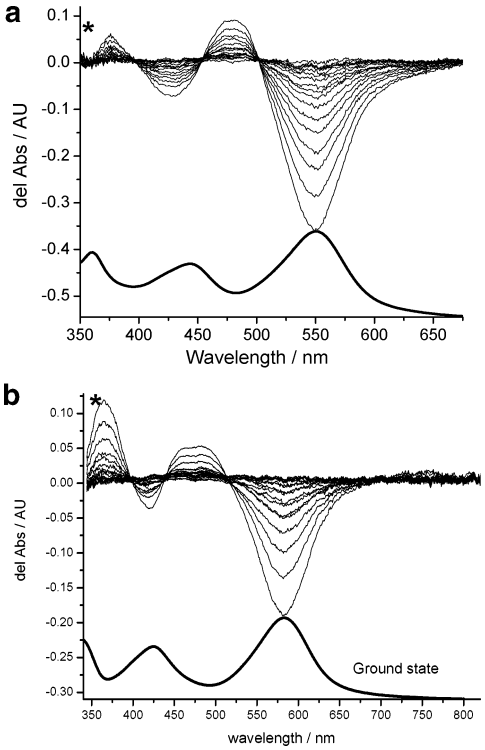

Figure 7. Ground-state and transient absorption spectra of (a) **1** (10 ns increment) and (b) $\mathbf{H_21}$ (5 ns increments), $\lambda_{exc} = 450$ nm. The asterisk indicates the 354.67 nm excitation line used in TR^2 and TR^3 experiments.

$\mathbf{H_21}$ are surprising, considering the larger differences observed in the ground-state spectra (Figure 6). The ground-state recovery time in each case is in close agreement with luminescence lifetimes, and the evolution of the spectra with time shows only a change in intensity, indicating that in both cases only a single excited-state species is present over the time range examined.

The combination of strong ground-state absorption at 350 and 530 nm and the presence of an excited-state absorption band at ~350 nm facilitates the study of **1** and $\mathbf{H_21}$ by transient (TR^2) and time-resolved resonance Raman spectroscopy (TR^3). Single-colored transient resonance Raman spectra were recorded in H_2O at both 354.67 and 532 nm for $\mathbf{1}/\mathbf{H_21}$ and $\mathbf{2}/\mathbf{H_22}$.

As shown in Figure 8, the presence of a significant ground-state as well as excited-state absorption (for both **1** and $\mathbf{H_21}$) at 354.67 nm enables the use of variation in the excitation laser pulse energy to differentiate between ground- and excited-state features. At low photon flux, the spectra are almost entirely composed of ground-state features at 1604, 1504, 1476, 1399, 1332, 1283, 1149, and 1016 cm^{-1} for **1** and at 1613, 1514, 1494, 1426, 1327, 1116, and 1005 cm^{-1} for $\mathbf{H_21}$. Excited-state resonance Raman spectra were obtained at higher photon flux.[41] Vibrational features typical of a bpy radical anion (at 1285 and

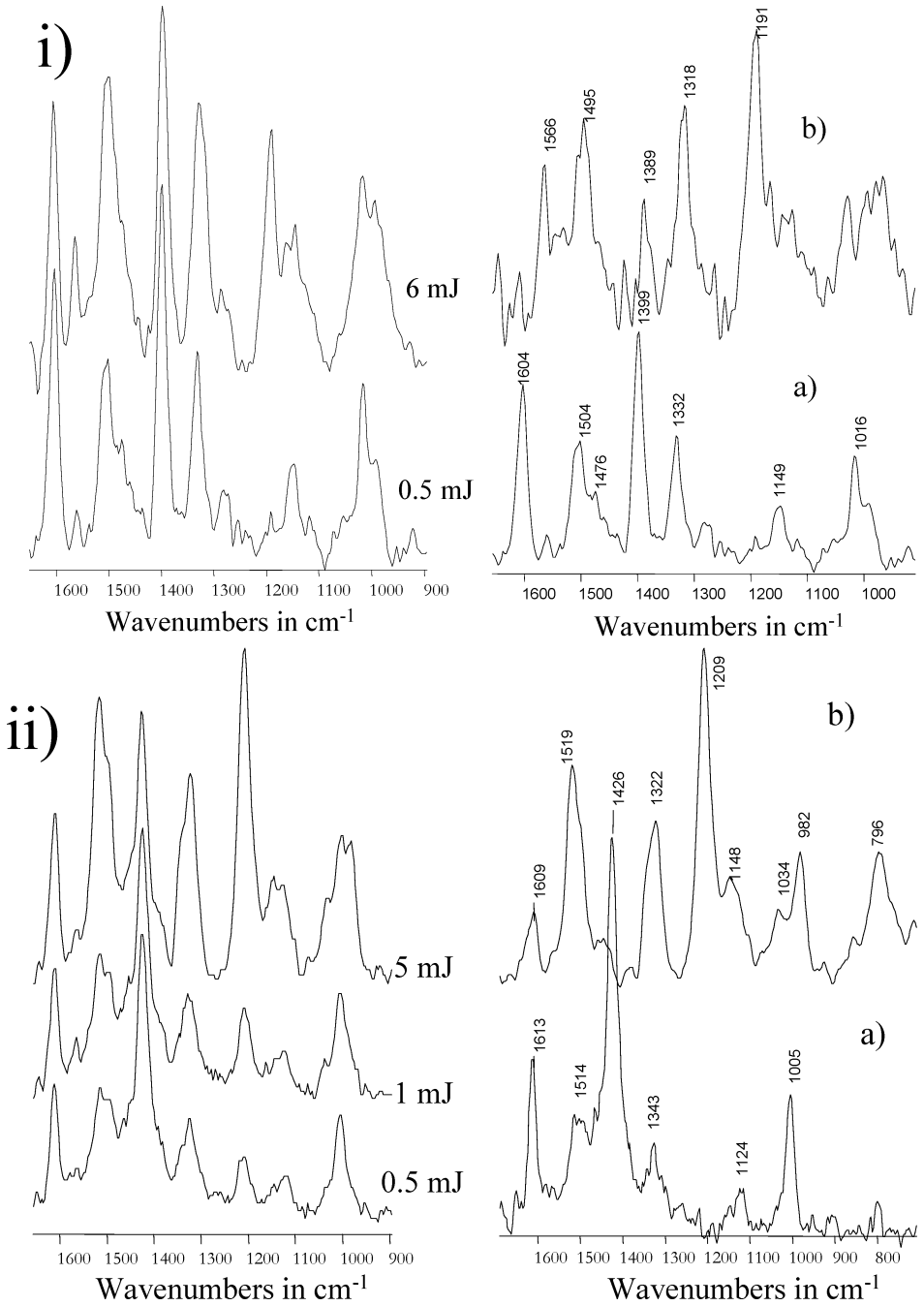

Figure 8. TR^2 spectra of (i) **1** and (ii) **$H_2$1** (in H_2O/HCl), single color pump and probe, λ_{exc} = 354.67 nm. Left: energy-resolved spectra normalized to ground-state feature. Right: (a) pure ground and (b) pure excited state.

1212 cm^{-1}) are notably absent in the high-energy TR^2 spectra of both **1** and **$H_2$1**. For **1**, excited-state bands are observed at 1566, 1495, 1389, 1318, and 1191 cm^{-1}. In the case of **$H_2$1**, the vibrational features appear at 1609, 1519, 1322, 1209, 1148, 982, and 796 cm^{-1}. Almost identical spectra were obtained for the deuterated analogues (**2**/**$H_2$2**), confirming that the peaks observed are pyrazine- rather than bpy-based. TR^2 spectra of **1** recorded at 532 nm show predominantly ground-state features, which are essentially identical to those obtained in the ground-state rR studies (vide supra). At high photon flux, bands at 1562, 1490, 1389, and 1320 cm^{-1} similar to those obtained at high photon flux at 354.67 nm are observed. For **$H_2$1**, only ground-state features are found, identical to rR spectra obtained by excitation at the same wavelength using a continuous-wave laser. This is in agreement with excited-state absorption spectra (vide supra), which indicates that insignificant excited-state absorption is present at 532 nm. Spectra recorded in acetonitrile-d_3 are in good agreement with the results obtained in aqueous solution. TR^3 spectra were recorded for both **1** and **$H_2$1** (λ_{pump} = 532 nm, λ_{probe} = 355 nm in H_2O; see Supporting Information, Figure S5). The time-resolved spectra obtained indicate, in agreement with the transient absorption spectra in Figure 7, the involvement of a single excited-state species (in the nanosecond time regime) in each case.

(41) Excited-state resonance Raman spectra: the resonance Raman spectra of the complex in its excited state with contributions to the spectra from the complex in the ground-state removed by spectral subtraction (see Figure 8).

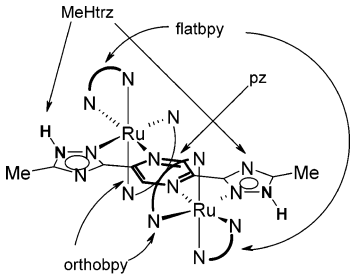

H_21

Figure 9. Nomenclature used in DFT calculations.

DFT Calculations. The complexes **1** and $\mathbf{H_21}$ were studied using the B3LYP/LanL2DZ functionals. As discussed above, both **1** and $\mathbf{H_21}$ are formed as homo- and heterochiral diastereoisomers; however, in the present study only the heterochiral stereoisomers are examined due to the significant simplification the presence of a center of symmetry brings to the calculation (Figure 9). For $\mathbf{H_21}$, an additional complication arises upon protonation. Previous studies on the relative reactivity of the uncoordinated nitrogen ligands of the 1,2,4-triazole ring have indicated that the N1 position is less acidic than the N4 position (Figure 1). Hence, the N1 position of each of the 1,2,4-triazoles was protonated for the DFT calculations of $\mathbf{H_21}$. After geometry optimization with an ultrafine integration grid, the molecular orbitals were broken down in terms of contributions from various groups in the molecule: *Ru*, the two Ru atoms; *pz*, the pyrazine ring; *Metrz*, the methyltriazole moieties (*MeHtrz* in the case of $\mathbf{H_21}$); *flatbpy*, the two equivalent bipyridines, which lie in the same plane, including the Ru−pz−Ru axis; and *orthobpy*, the remaining two bipyridines (Figure 9). The results obtained for the frontier orbitals of **1** and $\mathbf{H_21}$ are listed in Table S1 (Supporting Information).

In the frontier region, neighboring orbitals are often closely spaced. In such cases, consideration of only the HOMO and LUMO may not yield a realistic description. For this reason, partial density of states (PDOS) diagrams, which incorporate a degree of overlap between the curves convoluted from neighboring energy levels, can give a more representative picture. The PDOS diagrams for **1** and $\mathbf{H_21}$ are shown in Figure 10. Using the time-dependent density functional theory (TD-DFT) approach, the 35 lowest energy singlet transitions of **1** and $\mathbf{H_21}$ were calculated and are listed in Table S2 (Supporting Information). The results are simplified due to the presence of a center of symmetry, and the molecular orbitals of the complexes are either symmetric (A_g) or antisymmetric (A_u) with respect to the inversion center. Electronic transitions between orbitals of the same symmetry (labeled A_g in Table S2) are forbidden and have a calculated oscillator strength of 0; hence, only the A_u transitions arising from transitions between orbitals with differing symmetries contribute to the calculated UV−vis spectra (Figure 11). Electron density difference maps (EDDMs) corresponding to five electronic transitions discussed below are shown in Figure 11. These maps show the change in charge density associated with a particular electronic transition.

Discussion

The importance of the structure of the bridging ligand in determining the extent of intercomponent interaction in multinuclear transition metal polypyridyl complexes is well established.[2] Factors such as the distance between the metal centers, the nature of the bridge, and the electronic properties of the nonbridging components are of interest. In this contribution, the title compound has been designed to provide a closely related analogue for both the bpzt$^-$-type dimers (e.g., compound **4**, Figure 2) we have investigated in the past and the Creutz−Taube ion-type complexes. In the former case, the two metal centers are bridged by a ligand containing two pyrazine rings and directly bridging 1,2,4-triazole(s), while in the latter case the bridge is provided by a single pyrazine ring. The separation between the two metal centers is similar for the CT ion, **4**, and $\mathbf{1}/\mathbf{H_21}$, which allows examination of how the differences in the composition of the bridging ligand affect the electronic and electrochemical properties of the compounds. Of particular interest is the electron delocalization in the mixed-valence state and the effect that the protonation state of the triazole rings has on the electrochemical and electronic properties of the compound.

Redox Properties. The redox processes observed at anodic potentials for both **1** and $\mathbf{H_21}$ are assigned to sequential oxidation of each of the metal centers, and the separation (ΔE (**1**) = 175 mV, ΔE ($\mathbf{H_21}$) = 170 mV) is typical for complexes containing bridging pyrazine rings, such as $[(Ru(bpy)_2Cl)_2pz]^{2+}$ (ΔE = 130 mV)[5a] and $[(Ru(bpy)_2)_2dpp]^{2+}$ (ΔE = 200 mV).[6c] The ΔE value provides a measure for the stability of the mixed-valence compound toward disproportionation, as shown in eq 1, which yields values for the comproportionation constant, K_c, of 910 for **1** and 750 for $\mathbf{H_21}$.[42]

$$K_c = e^{\Delta E(\mathrm{mV})/25.69} \quad \text{at } T = 298 \text{ K} \tag{1}$$

The separation observed contains contributions from electrostatic interactions as well as electron delocalization.[43] The importance of the latter can be determined from a detailed analysis of the spectroscopic properties of the mixed-valence complexes. The observation of a very weak absorption band at 850 nm for $\mathbf{H_21}$ and the absence of an IT band in **1** indicates that, despite the proximity of the two metal centers, the electronic delocalization between the metal centers in the ground state is at best very weak and that the separation between the first and second redox processes is predominantly due to electrostatic contributions. Indeed, the strength of the effect is comparable with the electrostatic effect of protonation on the redox potentials of **1** and $\mathbf{H_21}$.[4c,44]

The electrochemical studies yield two unexpected results. First, while for both the CT ion and **4** electronic interaction (in terms of delocalization of the SOMO) is relatively strong, for $\mathbf{1}/\mathbf{H_21}$ electron delocalization is not significant. Second, it is unexpected that the value of ΔE obtained for $\mathbf{1}/\mathbf{H_21}$ is independent of the protonation state of the triazole ring. For other triazole-based dinuclear systems such as compound **5** (Figure 2), very different behavior is observed. In the depro-

(42) Richardson, D. E.; Taube, H. *Inorg. Chem.* **1981**, *20*, 1278−1285.
(43) Evans, C. E. B.; Naklicki, M. L.; Rezvani, A. R.; White, C. A.; Kondratiev, V. V.; Crutchley, R. J. *J. Am. Chem. Soc.* **1998**, *120*, 13096−13103.
(44) The effect of protonation can be viewed as a "double oxidation" in terms of the change in charge; therefore, the increase in the first and second redox potentials of **1** upon protonation to $\mathbf{H_21}$ would be expected to be equivalent to twice ΔE (i.e., 350 mV). The actual increase upon protonation is 400 mV, and the larger effect of protonation of the 1,2,4-triazole is probably due to the closer proximity of the increase in charge (and hence electrostatic effect) compared with oxidation of one metal center (cf. distance dependence of columbic interactions).

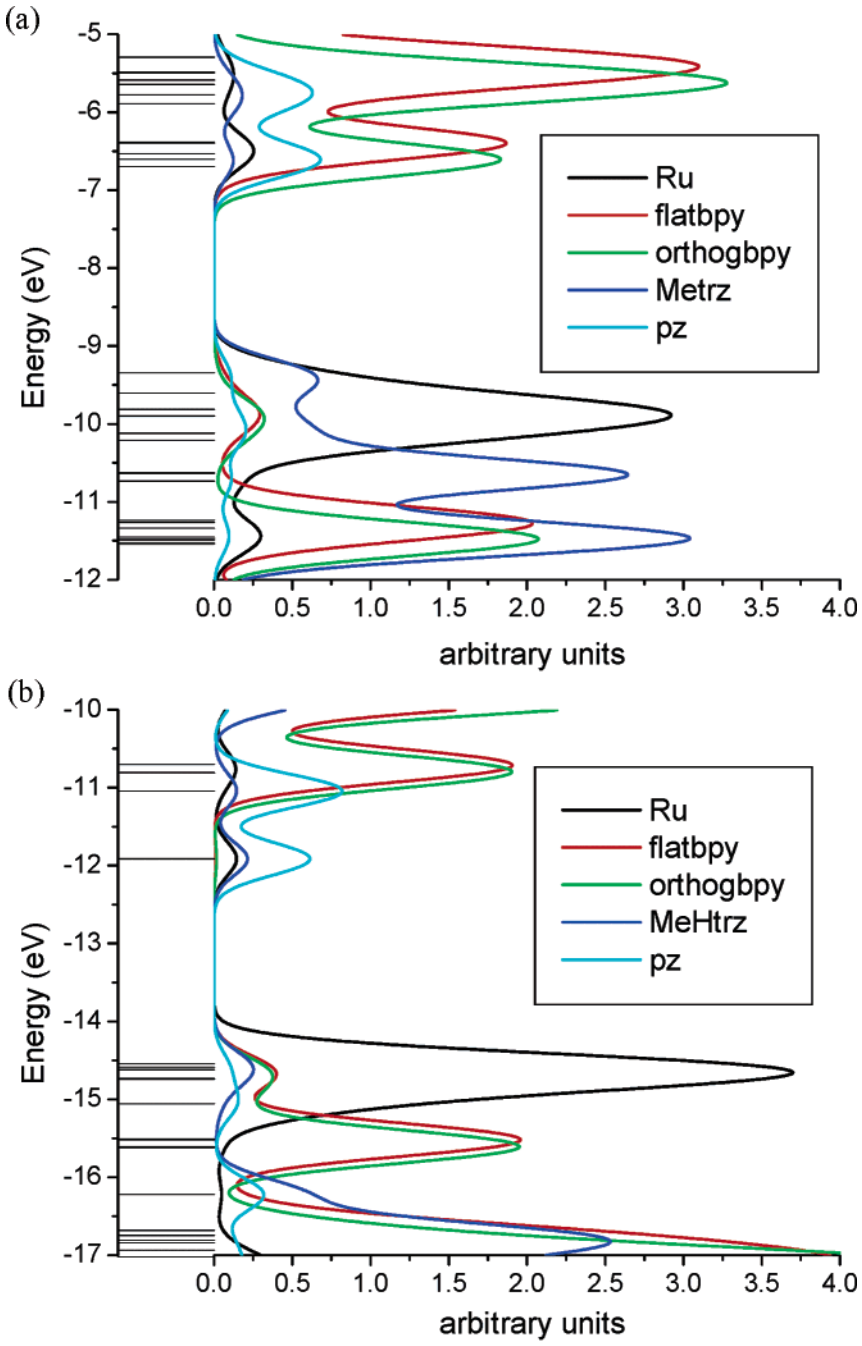

Figure 10. Partial density of states diagram for (a) **1** and (b) $\mathbf{H_2}$**1**. See text for description of the groups.

tonated state **5** shows a ΔE value of **170** mV, while for its protonated analogue a single two-electron wave is observed. In addition, for **5** the deprotonated analogue shows an intervalence band, while for the protonated species no intervalence features are observed. The pH-dependent behavior is typical of interaction via a hole-transfer mechanism[13] and is observed for related imidazole-based systems also.[45] It is, therefore, surprising that the ΔE values obtained for **1** and $\mathbf{H_2}$**1** are the same and that evidence for electron delocalization, in the form of an intervalence feature, is observed only for $\mathbf{H_2}$**1**. These observations make it very unlikely that hole transfer is an appropriate mechanism to describe the nature of the interaction between the two metal centers. However, the experimental observations may be explained by considering the strong coupling observed for the CT ion, which is rationalized by assuming a LUMO-mediated superexchange mechanism.[5] An important parameter, which determines the efficiency of such a mechanism, is the HOMO−LUMO energy gap. Meyer and co-workers have demonstrated that pyrazine-bridged binuclear complexes with better π-acceptor properties than NH_3 (e.g., $[(bpy)_2ClRu$-(μ-pyrazine)-$RuCl(bpy)_2]^{2+}$) exhibit a weaker IT band at much higher energy than the CT ion (Table 1).[5] The presence of good π-acceptor ligands, such as bpy, decreases the metal-based HOMO energy and hence increases the barrier to electron transfer between the Ru(II) and

(45) (a) Haga, M.; Ano, T.; Kano K.; Yamabe, S. *Inorg. Chem.* **1991**, *30*, 3843−3849 (b) Haga, M.; Ali, Md. M.; Koseki, S.; Fujimoto, K.; Yoshimura, A.; Nozaki, K.; Ohno, T.; Nakajima, K.; Stufkens, D. J. *Inorg. Chem.* **1996**, *35*, 3335−3347. (c) Haga, M.; Ali, Md. M.; Arakawa, R. *Angew. Chem., Int. Ed. Engl.* **1996**, *35*, 76−78.

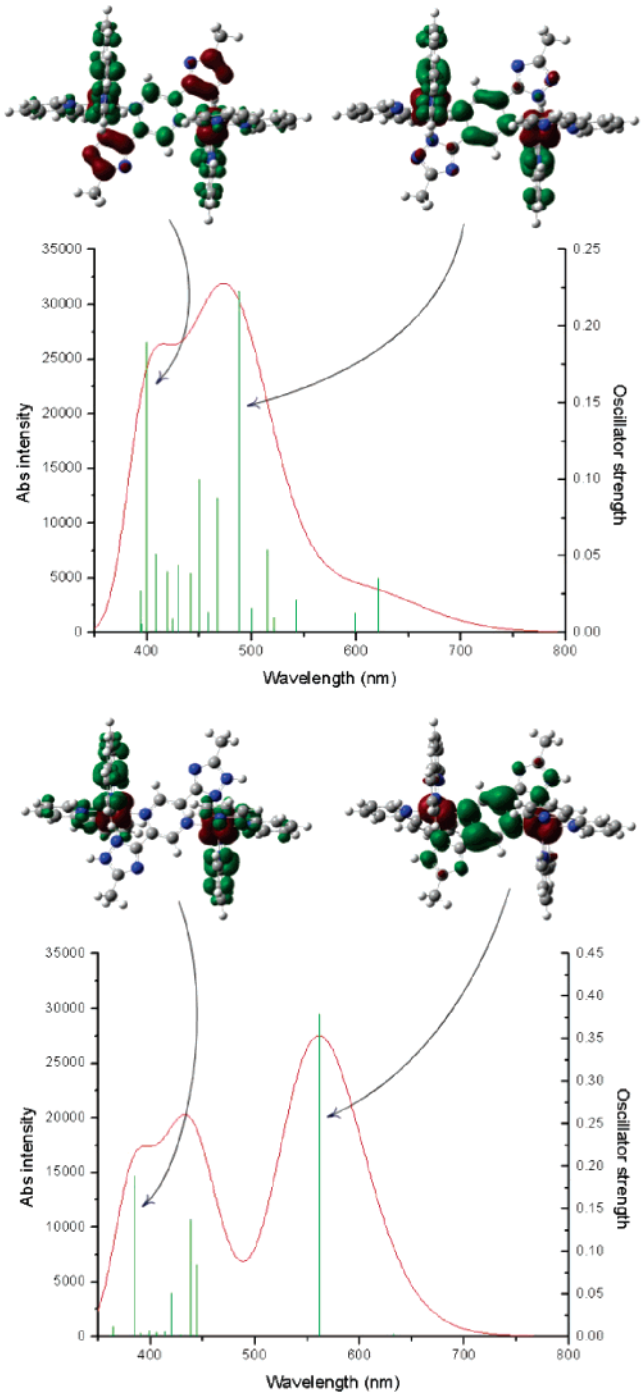

Figure 11. Convoluted calculated UV−vis spectrum of **1** (top) and $\mathbf{H_2}$**1** (bottom). The green lines are the individual electronic transitions. Also shown are three electron density difference maps corresponding to transitions 1, 13, and 30 (**1**) and 5, 8, and 25 ($\mathbf{H_2}$**1**) (green indicates an increase in the charge density, and red indicates a decrease).

Ru(III) centers. As a result, the oxidation of the first metal center affects the second metal center, but the barrier to electron "hopping" between the Ru(II) and Ru(III) centers is increased and the mixed-valence complex may be viewed as valence-trapped or localized.[4,46] Overall, the high energy barrier to optical electron transfer and the localization of the SOMO on a single metal center result in a lower oscillator strength and higher energy of the IT band than for the CT ion. If a LUMO-mediated exchange mechanism determines the intercomponent interaction in **1** and $\mathbf{H_2}$**1**, then the absence of a clear IT band in the mixed-valence state is not unexpected.

Reductive Processes. Assignment of the first reduction process observed at cathodic potentials as being pyrazine-based is made by comparison with closely related pyrazine-bridged binuclear complexes (Table 1). The subsequent reduction waves observed are assigned as bpy-based reductions, the first of which is a poorly resolved (ΔE < 60 mV) bielectronic redox wave corresponding, at least approximately, to a single bpy reduction of each metal center.[47] The third bpy reduction is at 200 mV more negative potential than the first/second bpy reduction. The third and fourth bpy reductions, which are again assigned to a single bpy reduction at each metal center, are separated by ~110 mV.

The observation that the first and second bpy reductions occur at almost the same potential, while there is a 110 mV separation between the third and fourth bpy reduction steps, may be rationalized on the basis that the first three bpy reduction steps are stabilized by delocalization over the remaining unreduced bpy ligands. For the fourth bpy reduction process, such stabilization is not available; hence, the separation (ΔE) between the third and fourth bpy reduction processes is larger than that between the first and second bpy reductions.[47]

The delocalization of charge in the reduced state is unexpected, considering the very low level of delocalization in the mixed-valence {Ru(II)Ru(III)} complexes (vide supra). If the "interaction" strength is a fixed parameter and is independent of the redox state of the complex, then four separate bpy reduction processes would be expected due to electrostatic factors, with the separation between the four bpy reductions being approximately equal.[48] The first two reductions are delocalized over eight pyridyl rings, and hence electrostatic interactions will be reduced significantly from those observed during oxidation where oxidation is localized on the ruthenium centers. The increased separation between the third and fourth reduction processes (100 mV) cannot be rationalized on the basis of a single reduction at each metal center since the electrostatic effect, and hence separation (ΔE), would be similar to that between the first and second bpy reduction processes. The increased separation can be explained by considering that the third reduction process is stabilized by delocalization over the two centers, while the last reduction does not benefit from such stabilization through delocalization. A similar reductive electrochemistry is seen in the related binuclear complexes $[(Ru(bpy)_2)_2bpt]^{3+}$ [14b] and $[(Ru(bpy)_2)_2bpzt]^{3+}$ [15] and indicates that there is significant interaction/delocalization between the bpy ligands on both metal centers. The results obtained suggest that the communication between the $Ru(bpy)_2^-$ units is increased when the bpy-based reductions are considered, and this can be explained by the fact that the bpy-based reductions take place in a complex containing a negatively charged (reduced) pyrazine

(46) (a) Hupp, J. T. *J. Am. Chem. Soc*. **1990**, *112*, 1563−1565. (b) Piepho, S. B. *J. Am. Chem. Soc*. **1990**, *112*, 4197−4206. (c) Petrov, V.; Hupp, J. T.; Mottley, C.; Mann, L. C. *J. Am. Chem. Soc*. **1994**, *116*, 2171−2172.

(47) Ghosh, B. K.; Chakravorty, A. *Coord. Chem. Rev.* **1989**, *95*, 239−294.

(48) The $E_{pc} - E_{pa}$ of the first bpy reduction peak is 120 mV and not the 29.5 mV expected for a double-electron-transfer process; 120 mV is twice that expected for an electrochemically reversible 1 e^- transfer. The third and fourth bpy reductions are electrochemically reversible ($E_{pc} - E_{pa}$ < 70 mV), and hence it is probable that the first and second reductions are also reversible, suggesting a separation of 60 mV between the first and second bpy reduction processes.

bridge and not a neutral bridge as is the case with oxidation processes.

Electronic Properties. The absorption spectra of **1**/**H$_2$1** contain three main absorption features in the visible region and are reminiscent of the spectra exhibited by related pyrazine-bridged binuclear complexes based on the ligands dpp[6c] and bpz (where bpz is 2,2′-bipyrazine).[36] Comparison of the absorption spectra of these compounds with those of **1**/**H$_2$1** suggests that the 550 nm band (Figure 4) is predominantly ^{1}MLCT (t_{2g} to pz) and the 450 nm band is ^{1}MLCT (t_{2g} to bpy) in character. This assignment is confirmed by resonance Raman spectroscopy and electrochemical data (vide supra). For **1**, a red shift in the 530 nm band to 565 nm and a blue shift of the 467 nm band to 424 nm are observed upon protonation.[13b] The red shift of the 530 nm band is most likely due to the stabilization of the pyrazine, which is supported by the DFT calculations (vide infra). Finally, the 350 nm absorption band is assigned, tentatively, as a pyrazine$-^1$IL ($\pi-\pi^*$) transition on the basis of the expected lower energy of the pyrazine$-\pi^*$ relative to the bpy$-\pi^*$. This assignment is supported by the pH dependence of the absorption band, which undergoes a blue shift on protonation (due to the concomitant lowering of electron density on the adjacent 1,2,4-triazole rings), and observation of pyrazine-based vibrational modes in the ground-state resonance Raman spectra obtained during TR^2 studies (vide supra) at $\lambda_{exc} = 355$ nm for both **1** and **H$_2$1**.

DFT Calculation. One of the central aims of the present study is to examine the effectiveness of DFT calculations in elucidating ground- and excited-state features in multinuclear complexes. The picture emerging from the spectroscopic and electrochemical measurements is that the LUMO in both **1** and **H$_2$1** is based on the pyrazine ligand and that, as expected, the HOMO is metal-based. The data indicate that both HOMO and LUMO are stabilized upon protonation. In this section the results obtained from the DFT calculations are compared with the experimental data.

The PDOS diagrams shown in Figure 9 suggest that for **1** the HOMOs are mainly *Ru*- and *Metrz*-based and the LUMOs are based on the bipyridines and *pz*. In contrast, the HOMOs of **H$_2$1** are almost completely *Ru*-based and the LUMOs are primarily based on *pz*, although there are also contributions from *MeHtrz* and *Ru*.

This can be visualized by the EDDM pictures shown in Figure 10a for **1**, which indicate that the lowest energy absorption (of significant oscillator strength) at 490 nm (transition 13, Table S2a; major contributions, H-4 → LUMO and H-2 → LUMO) corresponds to a transfer of electron density from *Ru* to *orthobpy* and *pz* (Figure 9). At ∼400 nm there is another electronic transition, also with high oscillator strength (transition 30). The major contributions are HOMO → L+7 and H-1 → L+6, and the change in charge density is similar to that calculated for transition 13. The energies observed for these main bands, as well as the absorption envelope, are quite different from the experimental results. Also, the results indicate a significant mixing of bpy and pz orbitals, in contradiction to resonance Raman data (vide supra). This apparent contradiction may be explained by consideration of the different environments for which the data are obtained. In the DFT calculations the complex is isolated (i.e., no solvation), while the rR experiments were carried out in aqueous solution. It is clear from the solvent dependence of the energy of the absorption bands at ∼400 and ∼550 nm that increasing solvent polarity (vide supra) also serves to increase the separation of the absorption bands (see Figure 6 and Figure S4).

In contrast, the calculated UV−vis spectrum of **H$_2$1** is in excellent agreement with experiment (Figure 11). For the protonated species, the lowest energy transition with a significant oscillator strength (transition 5, mainly H-1 → LUMO) corresponds to a transfer of electron density mainly from *Ru* to *pz*. Two transitions of similar oscillator strength contribute to the absorption band around 440 nm. The two transitions (transitions 7 and 8, containing different ratios of H-1 → L+1 and HOMO → L+1) correspond to very similar movements of electron density from *Ru* to *pz*. Another transition with a strong oscillator strength occurs at 385 nm. This transition (transition 25 in Table S2b) has a number of contributions, the largest of which are H-3 → L+3 and H-4 → L+2 and *Ru* to bipyridyl (mainly *orthobpy*) in nature. The DFT calculations for the protonated species therefore support the spectroscopic data. The lowest singlet excited state is pyrazine-based, and protonation of **1** leads to a decrease in the energy of the lowest ^{1}MLCT band.

The DFT calculations also support both the electrochemical observations and the mechanism proposed for the interaction between the metal centers in the mixed-valence state. They indicate that, for **1** and **H$_2$1**, the pyrazine moiety provides only very minor contributions to the HOMO and a large contribution to the LUMO, while the 1,2,4-triazoles provide a significant contribution to the HOMO. It is clear that the LUMO energy is stabilized to a greater extent than the metal-based HOMO levels upon protonation from **1** to **H$_2$1**. If the internuclear interaction is dominated by a LUMO-based superexchange mechanism, then an increase in the internuclear interaction would be expected, and although protonation has little effect on ΔE, the tentative observation of an IT band for **H$_2$1** and not for **1** suggests that a small increase in interaction occurs upon protonation.[4c]

Excited-State Electronic Structure and Properties. Although pyrazine-bridged complexes have been the focus of considerable attention for over half a century, the majority of the systems are nonemissive. It is generally accepted that the lowest excited states in those pyrazine-bridged systems, which are emissive (e.g. the dipyridopyrazine family of complexes), are pyrazine-based; however, few detailed studies have been carried out to confirm this.[6f] The emission spectra of **1** and **H$_2$1** are comparable with those reported for the related complexes (see Figure 2 and Table 1) $[Ru(bpy)_2(\mu\text{-}1Mepztr)Ru(bpy)_2Cl]^{3+}$ (**6**)[13e] and $[(Ru(bpy)_2)_3((pztr)_3ph)(Ru(bpy)_2Cl)_3]^{6+}$ (**8**).[49] The red shift observed upon protonation is in agreement with the stabilization of the pyrazine-based LUMO; however, assignment of the emitting state as pyrazine-based is not so clear since a significant isotope effect on the emission lifetimes for **1** and **H$_2$1** (at 298 and 77 K) is observed upon deuteriation of the bpy ligands (Table 1). In previous studies of heteroleptic complexes, deuteriation of the ligands on which the lowest excited state is based results in an increase in emission lifetime.[50] It would be expected, therefore, for **1** and **H$_2$1** that deuteriation of the bpy ligands should have no effect on the emission lifetime,

(49) Lempers, H. E. B.; Haasnoot, J. G.; Reedijk, J.; Hage, R.; Weldon, F. M.; Vos, J. G. *Inorg. Chim. Acta* **1994**, *225*, 67−74.
(50) Browne, W. R.; Vos, J. G. *Coord. Chem. Rev.* **2001**, *219*, 761−787 and references therein.

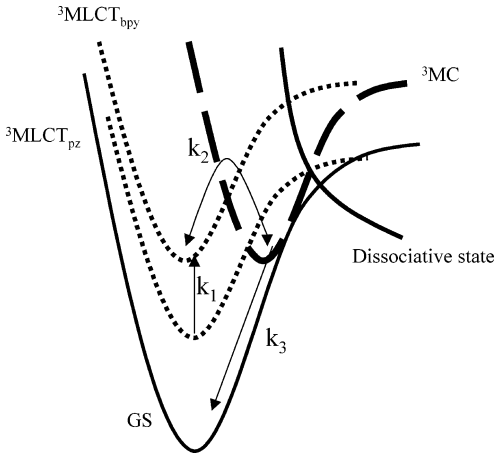

Figure 12. Excited-state internal conversion (IC).

as TR^2 and TR^3 studies strongly indicate that, for **1** and **H$_2$1**, the lowest excited state is pyrazine-based (i.e. the observation of features attributed to vibrations of the pyrazine group and the absence of the signature bands of the bpy anion radical 1212 and 1285 cm^{-1}).[37] The observation of a pronounced increase in the emission lifetime upon deuteriation of the bpy ligands is therefore somewhat surprising[50] but may be related to interaction between neighboring electronic states, one of which is bpy-based.

Interaction between close-lying, weakly coupled states is dominated by high-energy vibrational modes.[50,51] Hence, if the deactivation of the pyrazine-based ^{3}MLCT state via population of the higher bpy-based ^{3}MLCT state (Figure 12) is an important deactivation route, then the observation of a bpy deuteriation effect is possible. It is clear from the photochemical reactivity of **1** that the ^{3}MC state (thermal population of which is responsible for most ruthenium(II) polypyridyl photochemistry)[37] is accessible, and hence it is not unreasonable to assume that the higher energy ^{3}MLCT$_{bpy}$ states undergo rapid deactivation via this state. Considering Figure 12, if $k_1 \ll k_2 < k_3$, then the rate-determining step is the IC between the ^{3}MLCT$_{pz}$ state and ^{3}MLCT$_{bpy}$, in which, for weakly coupled states (i.e., with a Huang−Rhys factor $S < 1$), high-energy vibrational modes are important.[50,51] The absence of bpy anion radical features in the excited-state Raman data suggests that the lowest pyrazine ^{3}MLCT state is the only state that achieves a significant population at 298 K, and hence the bpy ^{3}MLCT state, if populated, must undergo rapid deactivation (e.g., via the ^{3}MC state, Figure 12). The rate of nonradiative decay of an excited state is the sum of several competing processes ($k_{obs} = k_{^3MLCT-GS} + k_1 + k_2 + k_3 + ...$), such as direct relaxation to the ground state and thermal population of a higher energy state. At 77 K, thermal population of the ^{3}MC state (k_2 in Figure 12) is not observed, and deactivation of the emissive ^{3}MLCT$_{pz}$ state via the weakly coupled ($S < 1$) ^{3}MLCT$_{bpy}$ state provides a proportionally larger contribution to k_{obs}; hence, the isotope effect would become larger.

Conclusions

Ground- and excited-state resonance Raman[41] and electrochemical data enable a detailed assignment to be made of the electronic absorption and emission spectra of **1** and **H$_2$1**. From the wavelength dependence of the rR spectra and electrochemistry, the absorption band at ca. 530 nm can be assigned as a

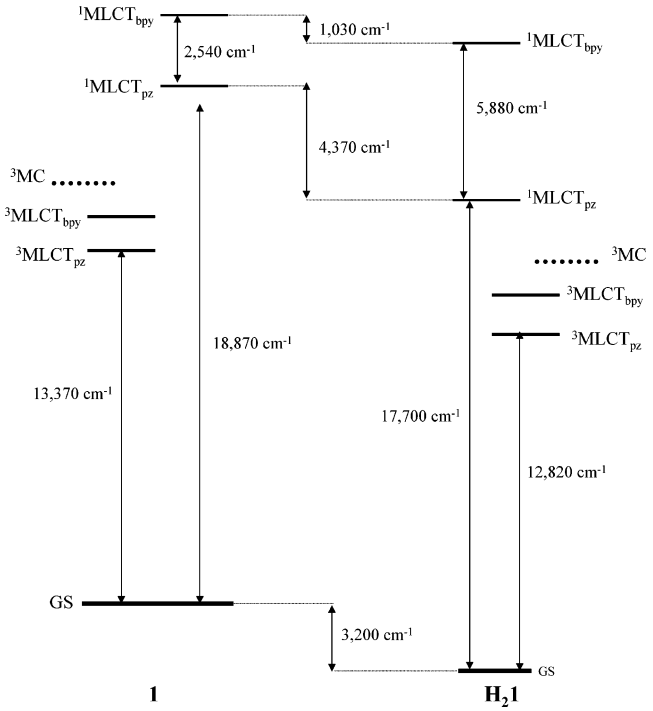

Figure 13. Diagram showing relative position of electronic states for **1** (left) and **H$_2$1** (right). Energy differences are estimated from spectroscopic and redox data.

$t_{2g}-\pi^*_{pz}$ ^{1}MLCT transition, the ca. 450 nm band is attributable to a $t_{2g}-\pi^*_{bpy}$ ^{1}MLCT transition, and the emission is assigned as arising from a pyrazine-based relaxed ^{3}MLCT state. A simplified electronic structure of both **1** and **H$_2$1** is represented in Figure 13. It is clear that, upon protonation, the lowest pyrazine-based ^{1}MLCT and ^{3}MLCT states are stabilized. In addition, due to the reduction in the σ-donor strength of the two triazole moieties, stabilization of the metal-based (t_{2g}) ground state and the photochemically active ^{3}MC (e_g) state also occurs. The electrochemical data suggest ground-state (HOMO) stabilization (Ru(II)/Ru(III) redox potential) by 3200 cm^{-1}, upon protonation, while electronic spectroscopy suggests that, upon protonation, the energy of the ^{1}MLCT$_{pz}$ band (and hence LUMO) is reduced by 4370 cm^{-1} and that of the ^{3}MLCT$_{pz}$ band is lowered by 3750 cm^{-1}.

In contrast to the ground state, which is stabilized by 3200 cm^{-1}, the bpy-based ^{3}MLCT states are relatively unaffected by protonation (stabilized by only 1030 cm^{-1}), and hence the effective GS-to-^{3}MLCT(bpy) energy gap is increased (Figure 13). It would be expected that a lowering in the energy of the ^{3}MC state would result in an increase in photochemical reactivity; however, the reverse is observed, with the deprotonated complex exhibiting photochemistry while the protonated complex is photochemically inert. Lowering of the ^{3}MC upon protonation reduces the energy gap between the ^{3}MC and ground state and hence leads to an increase in the rate of nonradiative

(51) (a) Hutchinson, C. A., Jr.; Mangum, B. W. *J. Chem. Phys.* **1960**, *32*, 1261−1262. (b) Wright, M. R.; Frosch, R. P.; Robinson, G. W. *J. Chem. Phys.* **1960**, *33*, 934−935. (c) Robinson, G. W.; Frosch, R. P. *J. Chem. Phys.* **1962**, *37*, 1962−1973. (d) Robinson, G. W.; Frosch, R. P. *J. Chem. Phys.* **1963**, *38*, 1187−1203. (e) Siebrand, W. *J. Chem. Phys.* **1967**, *46*, 440−447. (f) Siebrand, W. *J. Chem. Phys.* **1996**, *44*, 4055−4057. (g) Gelbart, W. M.; Freed, K. F.; Rice, S. A. *J. Chem. Phys.* **1970**, *52*, 2460−2473. (h) Jortner, J.; Rice, S. A.; Hochstrasser, R. M. *Adv. Photochem.* **1969**, *7*, 149−309. (i) Freed, K. F.; Jortner, J. *J. Chem. Phys.* **1970**, 52, 6272−6291. (j) Englman, R.; Jortner, J. *Mol. Phys.* **1970**, *18*, 145−148.

deactivation from the ^{3}MC to the ground state. This increase inhibits thermal population of a dissociative state from the ^{3}MC and hence inhibits photochemistry (Figure 12).

The incorporation of the acid−base chemistry of the 1,2,4-triazole moiety into the well-known Ru−pyrazine−Ru system has enabled the investigation of a pyrazine-bridged system which can undergo quite dramatic changes in both its ground- and excited-state properties, controllable by both solvent and pH. It is clear that the application of multiple techniques in a concerted manner to the elucidation of excited-state structure holds particular advantages, especially in determining the relative contributions of different ligand-based excited states to the electronic properties observed.

Acknowledgment. The authors thank Enterprise Ireland, the EU Framework 5 IHP Training Network Susana, Contract HPRN-CT-2002-00185, and the EPSRC (UK) GR/M45696 for financial support. K.L.R. acknowledges ANDOR Technology Ltd. for financial support. The authors thank Mr. Maurice Burke (DCU) for assistance in the recording of mass spectra.

Supporting Information Available: Detailed synthesis and experimental procedures; ^{1}H NMR spectrum of **1**; UV−vis spectra during photolysis of **1** in CH_3CN; rR spectra of $\mathbf{H_21}$ in H_2O; rR spectrum of **1** in CH_3CN; TR^3 spectra of **1**; eigenvalues, symmetry, and percent contribution of various groups (see text) for the frontier molecular orbitals of **1** and $\mathbf{H_21}$; calculated wavelengths and oscillator strength of the electronic transitions of **1** and $\mathbf{H_21}$. This material is available free of charge via the Internet at http://pubs.acs.org.

JA046034E